

Pre-optimization of hybridization ratio in hybrid excitation synchronous machines using electrical circuits modelling

Yacine Amara, S Hlioui, Hamid Ben Ahmed, Mohamed Gabsi

▶ **To cite this version:**

Yacine Amara, S Hlioui, Hamid Ben Ahmed, Mohamed Gabsi. Pre-optimization of hybridization ratio in hybrid excitation synchronous machines using electrical circuits modelling. Mathematics and Computers in Simulation, 2021, 184, pp.118-136. 10.1016/j.matcom.2020.04.024 . hal-03822385

HAL Id: hal-03822385
https://cnam.hal.science/hal-03822385

Submitted on 22 Mar 2023

HAL is a multi-disciplinary open access archive for the deposit and dissemination of scientific research documents, whether they are published or not. The documents may come from teaching and research institutions in France or abroad, or from public or private research centers.

L'archive ouverte pluridisciplinaire **HAL**, est destinée au dépôt et à la diffusion de documents scientifiques de niveau recherche, publiés ou non, émanant des établissements d'enseignement et de recherche français ou étrangers, des laboratoires publics ou privés.

Copyright

Version of Record: https://www.sciencedirect.com/science/article/pii/S0378475420301464
Manuscript_a11da4ace87af6313856fe2ca814ad66

Pre-optimization of hybridization ratio in hybrid excitation synchronous machines using electrical circuits modelling

Yacine Amara[1], Sami Hlioui[2], Hamid Ben Ahmed[3], Mohamed Gabsi[4]

[1] *Normandie Univ, UNIHAVRE, GREAH, 76600 Le Havre, France*
[2] *SATIE, UMR CNRS 8029, Conservatoire National des Arts et Métiers, Paris, France*
[3] *SATIE, UMR CNRS 8029, École normale supérieure de Rennes, 35170 Bruz, France*
[4] *SATIE, UMR CNRS 8029, École Normale Supérieure Paris-Saclay, 94230 Cachan, France*

Abstract

Hybridization ratio α is an additional degree of freedom offered by the hybrid excitation principle in the design of synchronous electrical machines. The first goal of this contribution is to present the tool developed for analysing the effect of the hybridization ratio. This software tool is based on the electrical circuits modelling of hybrid excitation synchronous machines. This tool can also be advantageously used for the pre-optimization of this parameter. The used model and the optimization algorithm are first thoroughly detailed. Finally, a parametric study intended to investigate the effect of some design specifications and parameters on this optimal value is presented.

Keywords: hybrid excitation, synchronous machines, permanent magnet, hybridization ratio, optimization, electric vehicles, efficiency.

1. Introduction

Hybrid excited synchronous machines (HESM) are synchronous machines where two magnetic excitation sources co-exist: permanent magnets (PM) and wound-field (WF) excitation. Thanks to this particularity, these machines possess an additional degree of freedom, which is the hybridization ratio α. This parameter reflects the contribution of PM to the total excitation flux. It can be advantageously exploited for the optimized design of electrical machines in very demanding applications [1].

The electric traction is chosen as the case study, in this contribution. For this application, the traction motor is often operating in partial load regions, which requires optimizing the power efficiency in these regions for achieving high energy efficiency. If classical synchronous machines are used, this additional requirement will be difficult to achieve without compromising other ones. Thanks to its additional degree of freedom HESM allow answering this new requirement without compromising others.

The value of α allowing optimizing efficiency around a given (Torque, Speed) operating point is determined thanks to an electrical circuits model based on first harmonics of the different quantities. Since this investigation only concerns the predesign of HESM, the parameters of adopted model are considered constant [2, 3]. More precise models could be adopted [4], but these require more complicated and time consuming approaches, which may not be necessary at the predesign stages. Nevertheless, the adopted model, even if it can be considered as too simple, is classical, widely spread and has been validated by many works [2, 3]. Furthermore, its exploitation in a parametric study helps answer this relative drawback.

This model is first introduced. Per-unit quantities are used in order to generalise the findings of this study. The algorithm allowing the determination of the optimal value of α is then detailed. Although already presented and used in a previous contribution [1], the software tool based on this algorithm has never been detailed. The first goal of this contribution is to present this tool, and allow the reader to replicate it. This tool, coded under MATLAB environment, is also made available through the link given as reference [5]. Finally, a parametric study intended to investigate the effect of some design specifications and parameters on this optimal value is presented. Variations of design parameters, mainly

© 2020 published by Elsevier. This manuscript is made available under the CC BY NC user license
https://creativecommons.org/licenses/by-nc/4.0/

resistances and inductances, could be due to, for example, temperature variations for resistances or magnetic saturation for inductances. This study will help analyse the effect of physical phenomena inherent to electrical machines operation on the hybridization ratio optimal value.

2. Pre-design model

The model used in this study is the classical, widely known first harmonic model for synchronous machines based on a synchronous *d–q* reference frame, including iron loss [1, 2, 3]. Figures 1(a) and 1(b) show equivalent circuits for armature windings, and Figure 1(c) shows an equivalent circuit for the wound field excitation. Steady state electric equations of this model could be easily derived from these figures [1, 3]. Symbols in these figures are defined as:

i_d, i_q *d* and *q* axes components of armature current,

I_e excitation current,

i_{fd}, i_{fq} *d* and *q* axes components of iron loss current,

v_d, v_q *d* and *q* axes components of terminal voltage,

V_e excitation coils terminal voltage,

R_a armature winding resistance per phase,

R_f iron loss resistance,

R_e excitation coils resistance,

Φ_a permanent magnet flux linkage,

Φ_{exc} total excitation flux linkage,

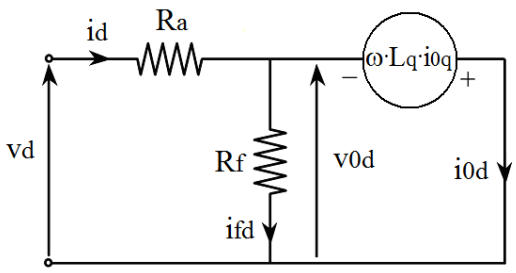
k_e "Armature/Excitation windings" mutual inductance,

L_d, L_q *d* and *q* axes components of synchronous inductance.

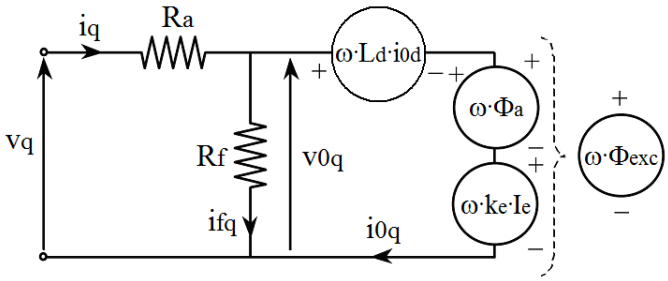
Thanks to the presence of the wound-field excitation, the total excitation flux varies with the excitation current; it can be expressed as

$$\Phi_{exc} = \Phi_a + k_e \cdot I_e = k_f \cdot \Phi_{e\,max}\,, \tag{1}$$

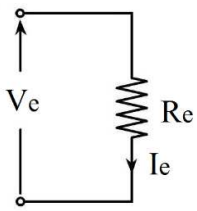
where, $\Phi_{e\,max}$ and k_f are the maximum total excitation flux and the excitation coefficient, respectively.



(a) *d* axis equivalent circuit



(b) *q* axis equivalent circuit



(c) Wound field excitation equivalent circuit

Fig. 1. Synchronous machines equivalent circuits model under motor mode operation.

The excitation coefficient varies ideally between 1, as an upper limit, and 0. Nevertheless, depending on how the HESM is designed, it may not be possible to completely cancel the excitation flux ($k_{f\,min} > 0$). Magnetic saturation, thermal limits or the demagnetization limit may set bound to the lower value of the excitation coefficient.

2.1. Per-unit system

Per unit system model allows a better understanding of parameters effect on machines performance. It is also a powerful tool for electric machines drives classification [6, 7, 8]. Base values of EMF and current are chosen as the rated values for the motor at rated speed (base speed Ω_b).

Per-unit values of the model parameters (resistances and inductances) are defined as

$$R_{an} = \frac{R_a \cdot I_m}{\Phi_{e\,max} \cdot p \cdot \Omega_b},\ R_{fn} = \frac{R_f \cdot I_m}{\Phi_{e\,max} \cdot p \cdot \Omega_b},\ R_{en} = \frac{R_e \cdot I_{em}}{V_{em}}, \tag{2}$$

$$L_{dn} = \frac{L_d \cdot I_m}{\Phi_{e\,max}},\ L_{qn} = \rho \cdot L_{dn},\ k_{en} = \frac{k_e \cdot I_{em}}{\Phi_{e\,max}}, \tag{3}$$

where,

p number of poles pairs,

I_m maximum armature current (in *d-q* referential),

I_{em} maximum excitation current,

V_{em} maximum excitation coils terminal voltage,

ρ saliency ratio.

Note the use of the subscript n to indicate per unit value. Per-unit values of excitation and armature currents and the armature terminal voltage are given by

$$I_n = \frac{\sqrt{i_d^2 + i_q^2}}{I_m},\ I_{en} = \frac{I_e}{I_{em}},\ V_n = \frac{\sqrt{v_d^2 + v_q^2}}{\Phi_{e\,max} \cdot p \cdot \Omega_b}. \tag{4}$$

Per-unit values of output power P, copper loss P_{Cu}, and iron loss P_{Fe} are given by

$$P_n = \frac{P}{V_m \cdot I_m},\ P_{Cun} = \frac{P_{Cu}}{V_m \cdot I_m},\ P_{Fen} = \frac{P_{Fe}}{V_m \cdot I_m}, \tag{5}$$

where, V_m is the maximum armature terminal voltage (in *d-q* referential). Finally, per-unit values of speed and torque are defined as

$$\Omega_n = \frac{\Omega}{\Omega_b},\ T_n = \frac{P_n}{\Omega_n}. \tag{6}$$

Another dimensionless parameter specific to synchronous machines with a wound field excitation, i.e., pure wound field excited synchronous machines and HESM, has also to be defined

$$\beta = \frac{V_m \cdot I_m}{V_{em} \cdot I_{em}}. \tag{7}$$

β is the power ratings ratio between converters supplying the armature and excitation windings, respectively. Hybridization ratio α, which is specific to HESM, is an additional degree of freedom from a design point of view; it is defined as

$$\alpha = \frac{\Phi_a}{\Phi_{e\,max}}. \tag{8}$$

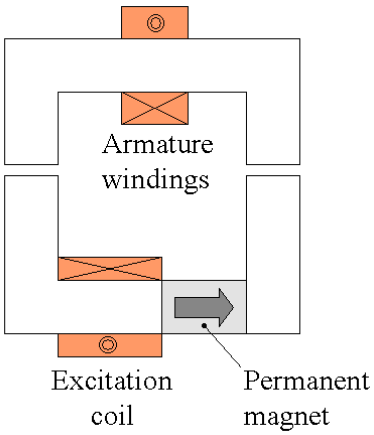
2.2. Hybridization ratio α

To illustrate this central parameter (hybridization ratio α) and its link with the design of HESM, examples of HESM structures combining PM and wound field excitations are presented in this sub-section.

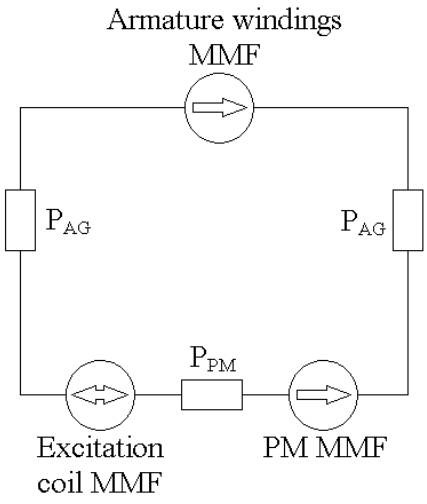
Different criteria can be used for classification of HESM [9, 10]. Two are specific to HESM: the first concerns the way the two magnetic excitation flux sources are combined, i.e., series and parallel hybrid excitation, and the second concerns the localization of excitation flux sources in the machine, i.e., both sources in the stator, both sources in the rotor and mixed localization. The first criterion is used here in order to illustrate the hybridization ratio α and how it can be adjusted.

Figure 2 illustrates the series hybrid excitation principle and two examples of structures belonging to this class. Figure 3 shows similar illustrations for the parallel hybrid excitation principle. In [10], a comparison between two machines belonging to each of the two classes has shown the superiority of the principle of parallel hybrid excitation. In fact, in series hybrid excitation, the flux generated by the wound-field excitation should cross the PM region which has a relatively high reluctance [10]. Flux control capability is then better for parallel HESM as compared to the series HESM.

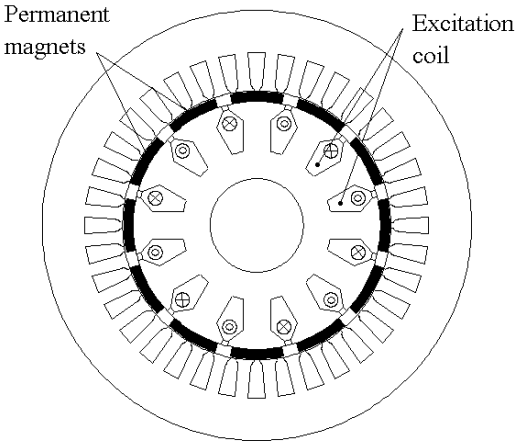
The hybridization ratio α, in these machines, could be adjusted by choosing adequate values of the parameters related to the PM and the wound-field excitation circuits, e.g. PM grade, PM thickness, number of turns of the wound-field excitation, and the excitation current limitations.



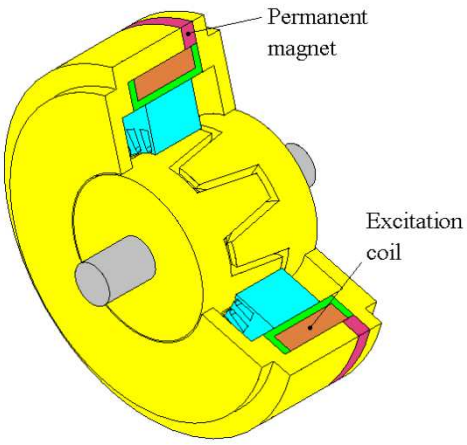
(a) Principle of series hybrid excitation



(b) Equivalent magnetic equivalent circuit

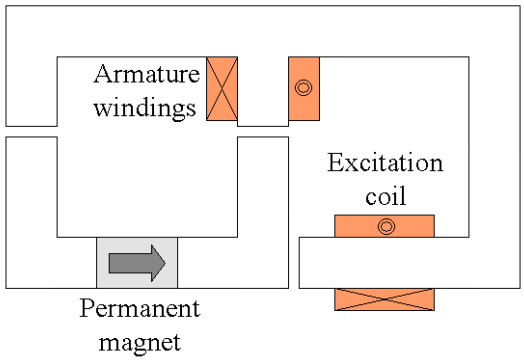


(c) 2D series HESM

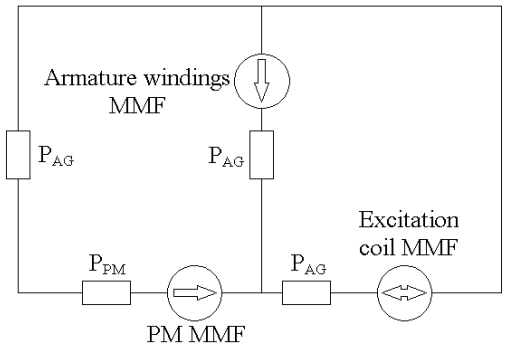


(d) 3D series HESM

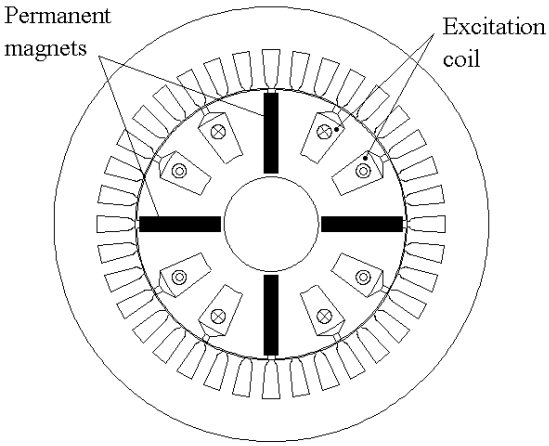
Fig. 2. Series HESM.



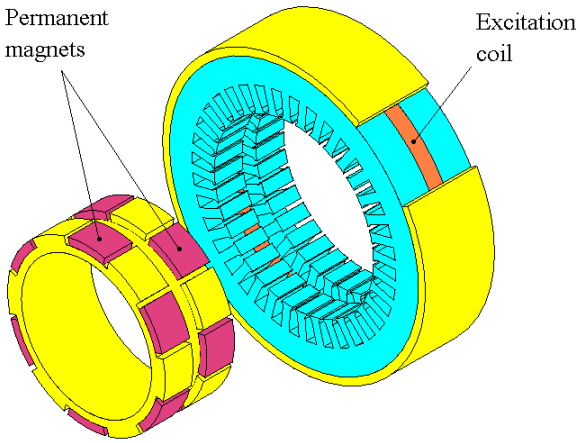
(a) Principle of parallel hybrid excitation



(b) Equivalent magnetic equivalent circuit



(c) 2D parallel HESM



(d) 3D parallel HESM

Fig. 3. Parallel HESM.

2.3. Optimization of hybridization ratio

HESM offers an additional degree of freedom in the control and design of synchronous machines as compared to other synchronous machines.

Electromagnetic loss in hybrid excited machines depends on two groups of parameters (9): one group corresponds to control parameters, the other one to design parameters.

$$P_{Cu} + P_{Fe} = f(\underbrace{I,\ \psi,\ k_f}_{\text{Control}},\ \underbrace{\alpha,\ L_d,\ \rho,\ \beta}_{\text{Design}}) \tag{9}$$

From the control point of view, hybrid excitation machines are similar to wound field synchronous machines [11]. From the design point of view, hybrid excitation machines have an additional degree of freedom, which is the hybridization ratio α [1].

Figure 4 shows an algorithm used to optimize hybridization ratio. This algorithm includes design and control parameters. It allows defining the value of hybridization ratio α which maximizes efficiency for desired "Speed – Torque" point (Ω_{n0}, T_{n0}). ψ is the phase shift between the armature current and EMF, and V_{nmax} is the normalized value of armature windings terminals maximum voltage.

This algorithm allows choosing, for α varying between 0 and 1, combinations of excitation coefficient k_f, normalized armature current I_n, and phase shift ψ, which maximizes efficiency η while respecting the voltage limit. Optimal value of hybridization ratio α_{opt} is the one which maximizes efficiency.

The entry data of this algorithm are the design specifications quantities (Ω_{n0}, T_{n0}). The design parameters or variables are embedded in the inner loop of this algorithm, i.e., the one allowing computing the efficiency. It is the first harmonic model which is used for that purpose. The design variables and their variations ranges are described in the next section "2.4".

The efficiency computation is at the heart of this optimization algorithm. It will be detailed in this section, and the files allowing the computation of efficiency maps are also provided along with this contribution [5]. Before starting describing the process allowing the computation of efficiency maps, it should be stressed that this algorithm has only been developed for non-salient machines, i.e., $\rho = 1$. Indeed, having $\rho = 1$ helps reducing the number of numerical computations, since some quantities required during the efficiency computation algorithm can be derived analytically, while having $\rho \neq 1$ requires these quantities to be determined numerically, which implies a longer computation duration. Nevertheless, explanations to extend it to salient poles machines are also provided.

The first aspect which should be given attention to is the fact that some parameters are interdependent regarding the way the per-unit system has been defined. Indeed, given the equation of excitation flux and its per-unit version (10), parameters k_{en}, normalized values of k_e, and β will be dependent on the value of hybridization ratio α. Equation (11) gives relations between these parameters and α. A detailed explanation of these relations is provided in Appendix A.

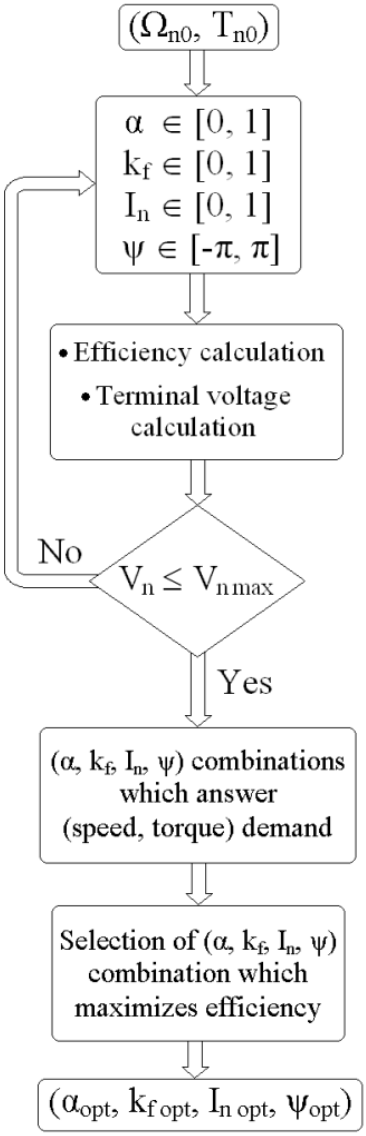


Fig. 4. Optimization algorithm.

$$k_f = \alpha + k_{en} \cdot I_{en} \tag{10}$$

$$\begin{cases} k_{en} = \begin{cases} \alpha & \text{if } \alpha \in [0.5,\ 1] \\ (1-\alpha) & \text{if } \alpha \in [0,\ 0.5] \end{cases} \\ \beta = \begin{cases} \beta_1 / \alpha^2 & \text{if } \alpha \in [0.5,\ 1] \\ \beta_1 / (1-\alpha)^2 & \text{if } \alpha \in [0.5,\ 1] \end{cases} \end{cases} \tag{11}$$

In equation (11), β_1 is the value of β when wound field excitation is only used for weakening the total excitation flux, i.e., $\alpha = 1$. The second step towards the computation of efficiency maps is the determination of the maximum normalized value of armature voltage V_{nmax}. The base speed should be first determined. The base speed is the maximum speed which could be reached while adopting the maximum torque control strategy. For non-salient poles machines ($\rho = 1$), the maximum torque is obtained when maximum excitation flux and maximum value of i_{0q} (Figure 1) [11], while respecting current limitation, are imposed. Figure 5 shows the algorithm used to compute V_{nmax}. A detailed explanation of this algorithm is provided in Appendix B. V_{nmax} computation should be done prior to any efficiency computation algorithm implementation.

Figure 6 shows the efficiency maps computation algorithm. This general algorithm could be applied for non-salient and salient poles machines. It allows to determine the maximum efficiency for a given (Ω_n, T_n) combination. Normalized torque can vary between 0 and 1 as a maximum value. Per-unit value of speed varies between 0 and $\Omega_{n\ \max} > 1$. For (Ω_n, T_n) combinations for which there is no means of respecting the voltage limit, the efficiency is set to 0 [1]. Mechanical losses are neglected in efficiency calculation, but they could be easily incorporated. The main problematic in this algorithm is the selection of (k_f , I_n, ψ) combinations.

This algorithm is different from the one shown in Figure 4, even if the efficiency computation is exactly similar in both, and it's at the heart of the two. The difference between them is their function. While the algorithm of Figure 4 is used for getting the optimal hybridization ratio for a given (Ω_{n0}, T_{n0}) combination (used for design purposes), the one shown in Figure 6 is used to generate the efficiency maps for the entire (Torque, Speed) plane, for a given machine, i.e., a given parameters combination.

The efficiency computation being at the heart of these two algorithms, the aim in what follows is to clearly explain the efficiency estimation methodology. Furthermore, in order to help the reader to replicate it, the algorithms, shown in Figures 4 and 6, are both made available through the link given as reference [5].

For non-salient poles machines, this problematic is simplified and many operations could be done analytically. For these machines, the selection of (k_f , I_n, ψ) combinations is done through four simple steps. These steps are explained here and further detailed in Appendix C. In fact, for each (Ω_n, T_n) combination, the selection process only requires the implementation of a single loop on k_f. The two other components (I_n, ψ) are determined analytically. The four steps are [12]:

1. analytical determination of i_{0dn} allowing maximizing efficiency for a given (Ω_n, T_n, k_f) combination;
2. analytical determination of i_{0dn} range allowing respecting current limitation ($I_n \leq 1$);
3. analytical determination of i_{0dn} range allowing respecting voltage limitation ($V_n \leq V_{nmax}$);
4. selection of (k_f , I_n, ψ) combination which maximizes efficiency.

The three first steps are independent, and can be processed in any order. In the fourth step, selection step, results of the three previous steps are exploited in order to select (k_f , I_n, ψ) combinations allowing maximizing efficiency, or set $\eta(\Omega_n, T_n) = 0$, if none of the (k_f , I_n, ψ) combinations are respecting current and/or voltage limitations.

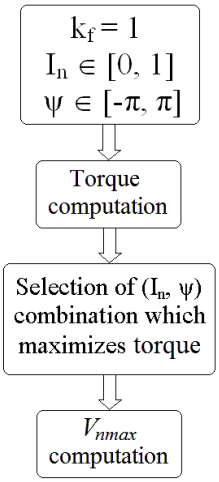


Fig. 5. V_{nmax} computation algorithm.

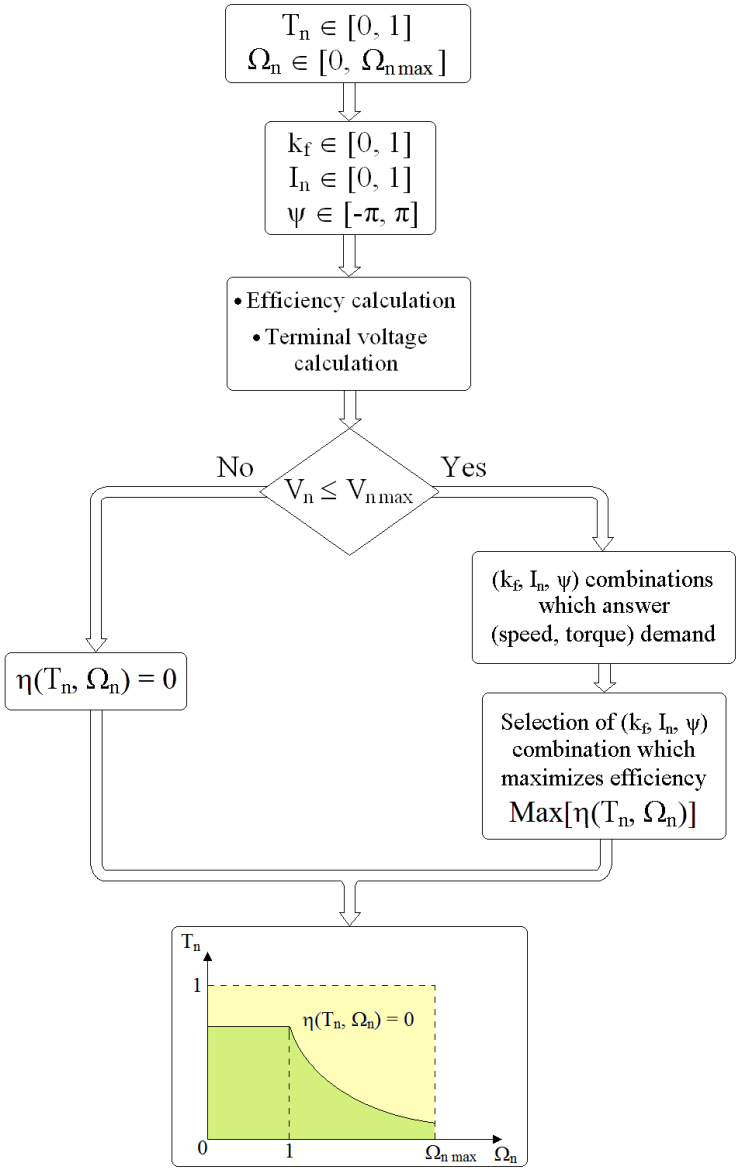


Fig. 6. Efficiency maps computation algorithm.

For the first step, it is possible to express the total normalized electromagnetic losses ($P_{Cun} + P_{Fen}$) as a function of i_{0dn}. The value of i_{0dn} allowing maximizing efficiency, for a given (Ω_n, T_n, k_f) combination, is obtained by finding the optimum of the losses function. This optimum is obtained for the value of i_{0dn0} given by (12) [2, 12]. More details are provided in Appendix C.

$$i_{0dn0} = \frac{-\Omega_n^2 \cdot L_{dn} \cdot \left(R_{an} + R_{fn}\right) \cdot k_f}{\left[R_{an} \cdot R_{fn}^2 + \Omega_n^2 \cdot L_{dn}^2 \cdot \left(R_{an} + R_{fn}\right)\right]} \tag{12}$$

For the second step, intervals for which the current limit is respected, if ever existing, are determined. This is done by solving equation $I_n \leq 1$, which corresponds to equation (13). Obtaining of this equation is explained in Appendix C [12].

$$\left[A_I \cdot i_{0dn}^2 + B_I \cdot i_{0dn} + C_I\right] \leq 0 \tag{13}$$

with,

$$\begin{cases} A_I = \left[1 + \left(\Omega_n \cdot L_{dn} / R_{fn}\right)^2\right] \\ B_I = 2 \cdot \left(\Omega_n^2 \cdot k_f \cdot L_{dn} \Big/ R_{fn}^2\right) \\ C_I = \left[\left(\left[\left(\Omega_n \cdot L_{dn} \cdot T_n \cdot V_{n\,max}\right)^2 + \left(T_n \cdot V_{n\,max} \cdot R_{fn} + \Omega_n \cdot k_f^2\right)^2\right] \Big/ \left(k_f \cdot R_{fn}\right)^2\right) - 1\right] \end{cases}$$

In case the discriminant of equation (13) is positive, let consider that it is verified for $i_{0dn} \in [i_{0dn1}, i_{0dn2}]$.

For the third step, intervals for which the voltage limit is respected, if ever existing, are determined by solving equation $V_n \leq V_{nmax}$, which corresponds to equation (14). Obtaining of this equation is explained in Appendix C [12].

$$\left[A_V \cdot i_{0dn}^2 + B_V \cdot i_{0dn} + C_V\right] \leq 0 \tag{14}$$

with,

$$\begin{cases} A_V = \left[L_{dn}^2 \cdot \Omega_n^2 \cdot \left[1 + \left(R_{an} / R_{fn}\right)\right]^2 + R_{an}^2\right] \\ B_V = 2 \cdot \Omega_n^2 \cdot k_f \cdot L_{dn} \cdot \left[1 + \left(R_{an} / R_{fn}\right)\right]^2 \\ C_V = \left[\begin{array}{l} \left(k_f \cdot \Omega_n \cdot \left(1 + R_{an} / R_{fn}\right) + \left(R_{an} \cdot T_n \cdot V_{n\,max} / k_f\right)\right)^2 \\ + \left(L_{dn} \cdot \Omega_n \cdot T_n \cdot V_{n\,max} \cdot \left(1 + R_{an} / R_{fn}\right) / k_f\right)^2 - V_{n\,max}^2 \end{array}\right] \end{cases}$$

In case the discriminant of equation (14) is positive, let consider that it is verified for $i_{0dn} \in [i_{0dn3}, i_{0dn4}]$.

The final step consists of finding, for a given (Ω_n, T_n) combination, the higher efficiency. In addition to outer loops allowing incrementing the speed and torque values, there is only one loop on k_f (inner loop). For a given set of k_f values, this loop will help identify values of (i_{0dn}, i_{0qn}), and subsequently (I_n, ψ), allowing to maximize efficiency. This loop will help to generate a vector containing efficiencies $\eta(k_f)$ corresponding to each value of k_f. Within this set of k_f values, the one which will be kept, at the end, is the one maximizing the efficiency. The following table (Table 1) describes what is principally done inside the

inner loop (loop on k_f), in order to estimate $\eta(k_f)$. More details are given in Appendix C, and files allowing the computation of efficiency maps could be downloaded from [5].

Table 1
Algorithm inside inner loop for a given (Ω_n, T_n, k_f) combination

Start
If discriminant of equation (13) is negative $\Rightarrow \eta(k_f) = 0$
Or if discriminant of equation (14) is negative $\Rightarrow \eta(k_f) = 0$
Else
If $[i_{0dn1}, i_{0dn2}] \cap [i_{0dn3}, i_{0dn4}] = \varnothing \Rightarrow \eta(k_f) = 0$
Else
If $i_{0dn0} \in [i_{0dn1}, i_{0dn2}] \cap [i_{0dn3}, i_{0dn4}] \Rightarrow \eta(k_f) = \eta(\Omega_n, T_n, k_f, i_{0dn0})$
Else $\eta(k_f) = \eta(\Omega_n, T_n, k_f, i_{0dn5})$, i_{0dn5} is equal to the intersection interval terminal which is closer to the value of i_{0dn0}.
End

2.4. Parameters variations

Table 2 gives normalized parameters variations intervals. These intervals are bounded by values between which the different parameters could reasonably vary. The two first lines, in this table, correspond to the design specifications quantities, and the rest to design variables.

The parametric study, presented in this contribution, is mainly conducted in order to establish the separate effects of each parameter on the optimal value of hybridization ratio. In addition to the effect of design specifications quantities (Ω_{n0}, T_{n0}), only losses parameters, within the design variables, are considered, i.e., R_{an} and R_{fn}. Several references [3, 6, 7, 8] have been analysed in order to establish reasonable variations intervals of the different parameters. Variations intervals, presented in Table 2, are chosen so as to include parameters found in these references. Authors of the reference [8] have identified some designs, 2 over 11 analysed designs, where the normalized values of armature windings resistance R_{an} are higher than 0.5. They pointed out that these designs correspond to small-power machines. It should be recalled that the machines concerned are these used for electric traction, which are classified within horsepower drives.

The initial values of the different design variables are given as follows: $L_{dn} = 0.5$; $\rho = 1$; $R_{an} = 0.1$; and $R_{fn} = 20$, $k_{en} = 1$; $R_{en} = 1$; $\beta = 27$, and $\alpha = 1$. These parameters have been derived from an existing prototype [1, 12, 13].

Table 2
Normalized parameters variations intervals

Parameter	Variations interval
Ω_{n0}	[0, 4]
T_{n0}	[0, 1]
L_{dn}	[0, 5]
ρ	[0, 5]
R_{an}	[0, 0.5]
R_{fn}	[5, +∞[
R_{en}	1
k_{en}	[0, 1]
β	[5, +∞[

3. Design specifications and variables effects

The effects are evaluated using drawings of isovalues of some quantities, efficiency among others, on the (Torque, Speed) plane.

As explained earlier, the chosen hybridization ratio α_{opt} allows efficiency maximization in a given (Torque, Speed) region. This efficiency is evaluated by neglecting mechanical losses, and it does not include the static converter losses.

Figure 7 shows the efficiency map of the HESM with previously defined parameters. Efficiency maps constitute a convenient way to assess motor designs and their control strategies [1, 4, 11, 12, 14, 15, 16, 17, 18, 19, 20, 21, 22, 23]. Effects of the different parameters and variables are studied in the following sections.

3.1. Design specifications

In order to investigate the design specifications effects on the value of optimal hybridization ratio α_{opt}, a first optimization study is conducted. The optimization algorithm has been used in order to determine the value of α allowing maximizing the efficiency for (Ω_{n0} = 2, T_{n0} = 0.2). It has been found that α_{opt} should be equal to 0.5.

Figure 8 shows efficiency maps for previous machine with a modified value of hybridization ratio, i.e., α = 0.5. As can be seen, the adoption of this new hybridization ratio allowed to shift the high efficiency zone to the desired operating (Ω_{n0}, T_{n0}) point [1] [22].

In order to investigate the separate effects of speed and torque on the value of optimal hybridization ratio, a first study is conducted by keeping the speed Ω_{n0} constant (Ω_{n0} = 2) and varying the torque value T_{n0} (Figure 9), and then keeping the torque constant (T_{n0} = 0.2) and varying the speed value Ω_{n0} (Figure 10). The value of optimal hybridization ratio is decreasing as the torque T_{n0} is decreasing for a constant speed, or as the speed Ω_{n0} increases for a constant value of T_{n0}. Figure 11 shows isovalues of α_{opt} in the (Torque, Speed) plane.

For Figure 9, the optimal hybridization ratio variations stop for a value of $T_{n0} \approx 0.433$, because beyond this value the machine is not able to deliver a torque while respecting current or/and voltage limits.

Obtained results are logical and conform to the electrical machines general behaviour. Indeed, for high values of torque it would be logically better to produce excitation flux from permanent magnets and therefore having minimum copper losses. For high speed operation where both the iron and copper losses may be significant, the flux weakening is made easier as the PM flux is reduced.

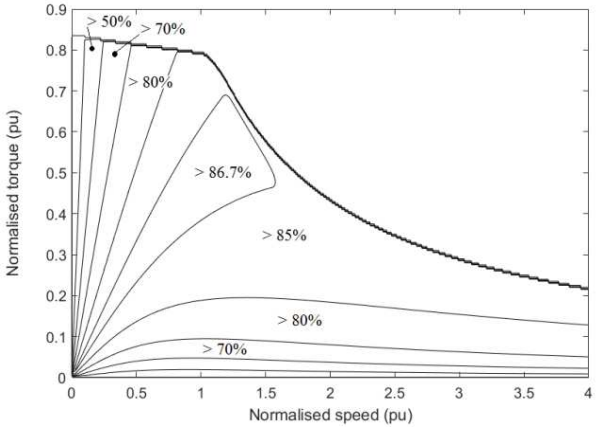


Fig. 7. Efficiency map of the HESM (α = 1).

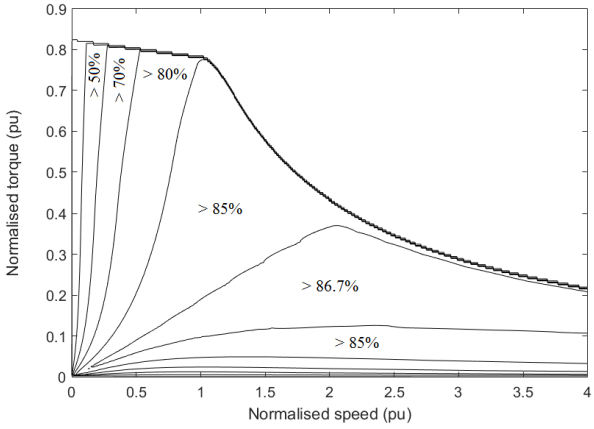


Fig. 8. Efficiency map of the HESM (α = 0.5).

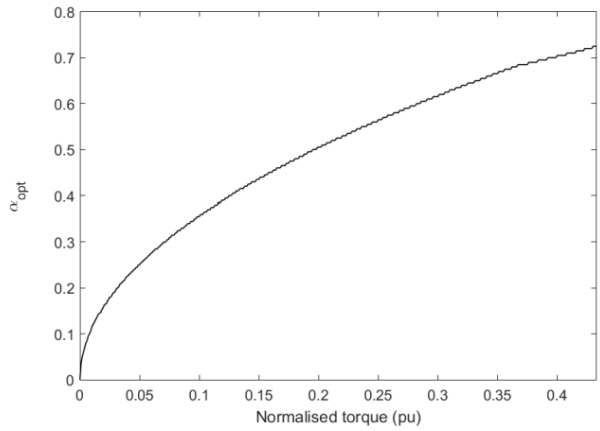


Fig. 9. Optimal hybridization ratio for $\Omega_{n0} = 2$.

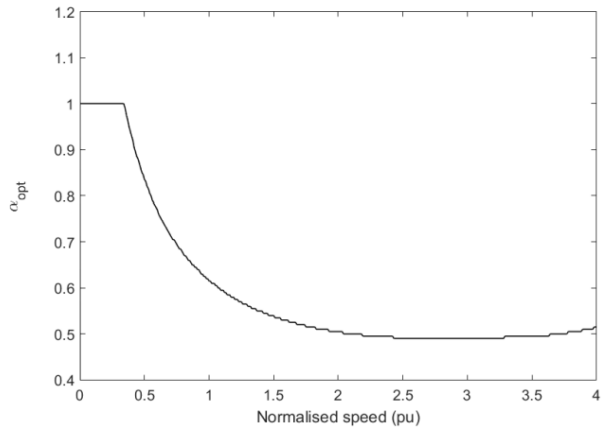


Fig. 10. Optimal hybridization ratio for $T_{n0} = 0.2$.

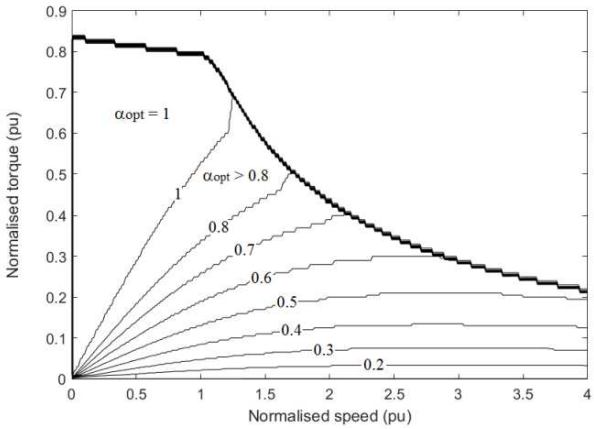


Fig. 11. Isovalues of α_{opt} in the (Torque, Speed) plane.

3.2. Design variables

As stated earlier, in section "2.4", only losses parameters, within the several design variables, are considered, i.e., R_{an} and R_{fn}, in this sensitivity study. Effects of these parameters are studied separately. For that purpose, curves shown in Figures 9 and 10 are plotted for different values of R_{an} and R_{fn}. Figures 12 and 15 show variations of the optimal hybridization ratio for different values of R_{an} and R_{fn}, respectively.

Figure 12(a) shows variations of optimal hybridization ratio, when $\Omega_{n0} = 2$, for three values of normalized armature resistance R_{an}, while R_{fn} is kept constant ($R_{fn} = 20$). It could be noticed that, for a large torque range when this resistance is higher the optimization algorithm tends to give a higher value of α_{opt}, which is quite coherent since the efficiency is higher when torque production is mainly insured by PM excitation flux. The curves stop at a given normalized torque value, which vary with R_{an}, because beyond this value the torque production could not be insured while respecting the current and/or the voltage limits. The machine could produce higher torque as the armature joule losses are lower (lower values of R_{an}). The value of α_{opt} is higher when $R_{an} = 0$, for $T_{n0} < 0.1$, is mainly due to the fact that under a certain value of R_{an}, the armature joule losses are so low, that the torque could be insured with the minimum iron loss, by imposing a large armature current in d axis while opposing PM excitation flux (flux weakening operation).

In order to further investigate this phenomenon, variations of optimal values of different design and control quantities, i.e., hybridization ratio α (Figure 13), and armature current amplitude I_n [Figure 14(a)] and phase-shift ψ [Figure 14(b)], with R_{an}, when ($\Omega_{n0} = 2$, $T_{n0} = 0.05$), have been computed. Figures 13 and 14 show these variations and it could be seen that for low values of R_{an}, the optimization algorithm

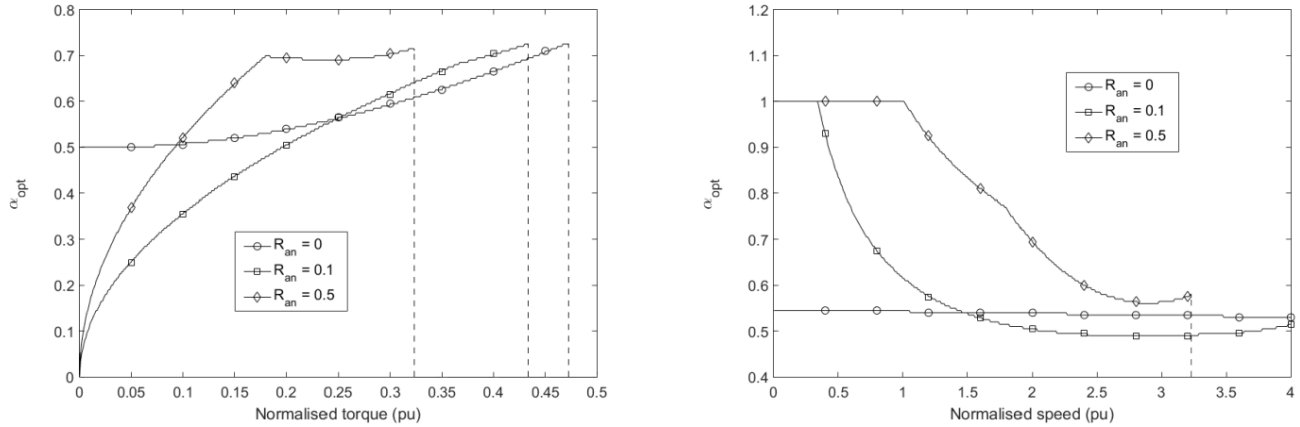
imposes a flux weakening operation [Figures 14(a) and 14(b)]. It should also be noticed that this type of operation is limited to a narrow variation range of low values of R_{an} (Figure 13).

When $T_{n0} = 0.2$ [Figure 12(b)], the value of α_{opt} is higher as armature joule losses are higher. The torque $T_{n0} = 0.2$ could not be maintained beyond a certain speed ($\Omega_{n0} \approx 3.2$) for the machine with $R_{an} = 0.5$. For the machine with $R_{an} = 0$, the optimal value of the hybridization ratio is relatively constant ($\alpha_{opt} \approx 0.55$). The torque production for this machine should be insured by the PM to reduce excitation joule losses.

Figures 15(a) and 15(b) show similar variations as Figures 12(a) and 12(b) respectively, but it is R_{fn} which varies this time, while R_{an} is kept constant ($R_{an} = 0.1$). It can be noticed from Figure 15(a), that when the iron loss could be neglected (higher values of R_{fn}), the algorithm tends to give a higher value of α_{opt}.

Indeed, when iron loss could be neglected, it is more convenient to produce the torque by increasing the excitation flux and reducing the electrical load (armature current). The torque production is improved as the iron losses are getting lower. For machines with $R_{fn} = 5$ and $R_{fn} = 20$, the optimization algorithm gives more or less same values of α_{opt}.

Figure 15(b) shows variations of optimal hybridization ratio, when $T_{n0} = 0.2$. As previously, the algorithm tends to give a higher value of α_{opt} when iron losses could be neglected. This is again quite coherent. When the speed increases, the optimal value of hybridization ratio is decreasing, to lessen iron loss and allow an easier flux weakening operation. The torque $T_{n0} = 0.2$ could not be maintained beyond a certain speed ($\Omega n0 \approx 3.6$) for the machine with $R_{fn} = 5$.



(a) $\Omega_{n0} = 2$ (b) $T_{n0} = 0.2$

Fig. 12. Optimal hybridization ratio variations for different values of R_{an}.

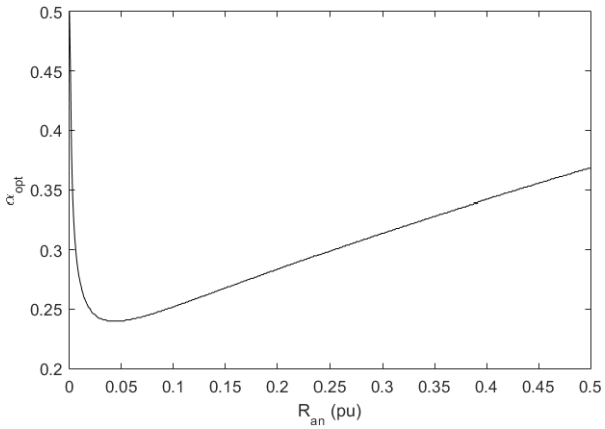
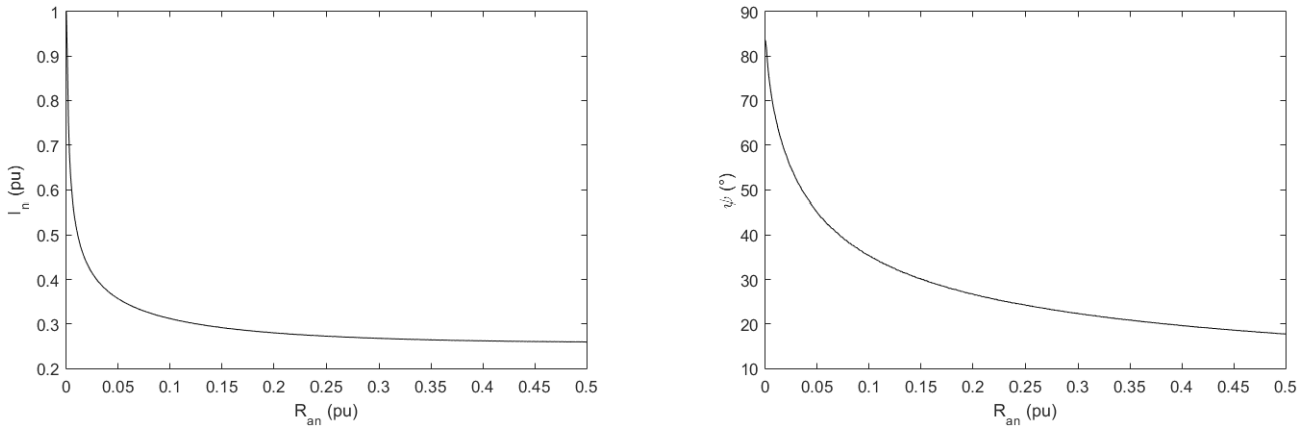
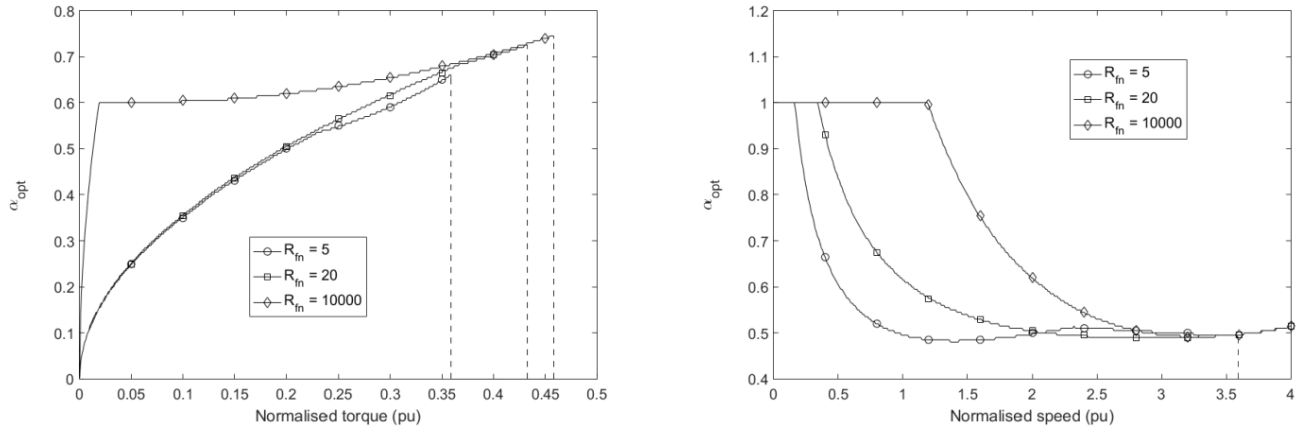


Fig. 13. Optimal hybridization ratio α_{opt} variations with R_{an} for ($\Omega_{n0} = 2$, $T_{n0} = 0.05$).



(a) (b)

Fig. 14. Optimal values of I_n (a) and ψ (b) variations with R_{an} for ($\Omega_{n0} = 2$, $T_{n0} = 0.05$).



(a) $\Omega_{n0} = 2$ (b) $T_{n0} = 0.2$

Fig. 15. Optimal hybridization ratio variations for different values of R_{fn}.

4. Conclusions

The study presented in this contribution helped assessing the validity and efficacy of the algorithm allowing the computation of optimal hybridization ratio. The efficiency computation, which is at the heart of this algorithm, has been detailed, to allow the reader to replicate it. This algorithm has proven to be reliable, and has been used to analyse the effect of design specifications and variables on α_{opt}. The parametric study undertaken has clearly shown the usefulness of the developed tool. This tool could be used for both design and analyses purposes, as has been seen in sections "3.1" and "3.2". This quantitative study, related to the pre-optimization of the hybridization ratio, has shown that the results are consistent with the physics of electric machines. Furthermore, no contradictions with previous literature were found, which comfort the trust on the developed algorithms.

This tool will be further improved in order to reduce simplifying assumptions on which the used model of HESM is based. The next steps will be to consider salient poles machines, and include a consideration of the magnetic saturation. Nevertheless, the presented tool has clearly showed how the additional degree of freedom, offered by the HESM, could be advantageously used to optimize the energy efficiency of electric drives used in electric vehicles.

References

[1] Y. Amara, L. Vido, M. Gabsi, E. Haong, A. H. Ben Ahmed, M. Lécrivain, Hybrid excitation synchronous machines: Energy-efficient solution for vehicles propulsion, IEEE Trans. Veh. Technol. 58 (2009) 2137–2149.

[2] S. Morimoto, Y. Tong, Y. Takeda, T. Hirasa, Loss minimization control of permanent magnet synchronous motor drives, IEEE Trans. Ind. Electron. 41 (1994) 511–517.

[3] F. Fernandez-Bernal, A. Garcia-Cerrada, R. Faure, Determination of parameters in interior permanent-magnet synchronous motors with iron losses without torque measurement, IEEE Trans. Ind. Appl. 37 (2001) 1265–1272.

[4] M. H. Mohammadi and D. A. Lowther, A computational study of efficiency map calculation for synchronous AC motor drives including cross-coupling and saturation effects, IEEE Trans. Magn. 53 (2017) paper 8103704.

[5] https://drive.google.com/file/d/1sttxS6x7B3QACbqyT2-_s70sgnL26GNt/view?usp=sharing

[6] R. F. Schiferl, T. A. Lipo, Power capability of salient pole permanent magnet synchronous motors in variable speed drive applications, IEEE Trans. Ind. Appl. 26 (1990) 115–123.

[7] W. L. Soong, T. J. E. Miller, Field-weakening performance of brushless synchronous AC motor drives, IEE Proc.-Electr. Power Appl. 141 (1994) 331–340.

[8] J. Soulard, B. Multon, Maximum power limits of small single-phase permanent magnet drives, IEE Proc.-Electr. Power Appl. 146 (199) 457–462.

[9] Y. Amara, J. Lucidarme, M. Gabsi, M. Lécrivain, A. H. Ben Ahmed, and A. Akémakou, A new topology of hybrid synchronous machine, IEEE Trans. Ind. Appl. 37 (2001) 1273–1281.

[10] Y. Amara, S. Hlioui, R. Belfkira, G. Barakat, and M. Gabsi, Comparison of open circuit flux control capability of a series double excitation machine and a parallel double excitation machine, IEEE Trans. Veh. Technol. 60 (2011) 4194– 4207.

[11] Y. Amara, S. Hlioui, H. Ben Ahmed, M. Gabsi, Power capability of hybrid excited synchronous motors in variable speed drives applications, IEEE Trans. Magn. 55 (2019) 8204312.

[12] Y. Amara, Contribution à la conception et à la commande des machines synchrones à double excitation. Application au véhicule hybride, Ph. D. Thesis manuscript, UNIVERSITE PARIS XI, 2001, France, Français (French).

[13] Y. Amara, E. Hoang, M. Gabsi, M. Lécrivain, A. H. Ben Ahmed, S. Dérou, Measured performances of a new hybrid excitation synchronous machine, EPE Journal 12 (2004) 42–50.

[14] S. S.Williamson, S. M. Lukic, A. Emadi, Comprehensive drive train efficiency analysis of hybrid electric and fuel cell vehicles based on motorcontroller efficiency modeling, IEEE Trans. Power Electron. 21 (2006) 730–740.

[15] Y. Sugii, M. Yada, S. Koga, T. Ashikaga, Applicability of various motors to electric vehicles, in Proc. 13th Int. EVS, Osaka, Japan, Oct. 1996, pp. 757–764.

[16] A. Fonseca, C. Chillet, E. Atienza, A.-L. Bui-Van, J. Bigeon, New modelling methodology for different PM motors for electric and hybrid vehicles, in Proc. IEEE Int. Electr. Mach. Drives Conf., Cambridge, MA, Jun. 2001, pp. 173–178.

[17] M. Menne, J. Reinert, R. W. De Doncker, Energy-efficiency evaluation of traction drives for electric vehicles, in Proc. 15th EVS, Brussels, Belgium, Oct. 1998, 7 pages, CD-ROM.

[18] L. Vido, M. Ruellan, Y. Amara, M. Gabsi, and H. Ben Ahmed, Recherche des paramètres optimaux d'une machine synchrone à aimants permanents, Eur. J. Electr. Eng. 2–3 (2011) 135–163.

[19] W. Q. Chu, Z. Q. Zhu, J. Zhang, X. Liu, D. A. Stone, and M. P. Foster, Investigation on operational envelops and efficiency maps of electrically excited machines for electrical vehicle applications, IEEE Trans. Magn. 51 (2015) paper 8103510.

[20] Z. Q. Zhu, W. Q. Chu, and Y. Guan, Quantitative comparison of electromagnetic performance of electrical machines for HEVs/EVs, CES Transactions on Electrical Machines and Systems 1 (2017) 37–47.

[21] H.-C. Jung, G.-J. Park, D.-J. Kim, and S.-Y. Jung, Optimal design and validation of IPMSM for maximum efficiency distribution compatible to energy consumption areas of HD-EV, IEEE Trans. Magn. 53 (2017) paper 8201904.

[22] A. S. Mohammadi, J. P. Trovão, and M. R. Dubois, Hybridisation ratio for hybrid excitation synchronous motors in electric vehicles with enhanced performance, IET Electr. Syst. Transp. 8 (2017) 12–19.

[23] C. T. Krasopoulos , M. E. Beniakar, and A. G. Kladas, Multicriteria PM motor design based on ANFIS evaluation of EV driving cycle efficiency, IEEE Trans. Transport. Electrific. 4 (2018) 525–535.

Appendix A

Within the hybridization ratio variation range $\alpha \in [0, 1]$, three domains could be identified: $\alpha = 1$, $\alpha \in]1, 0.5]$, and $\alpha \in]0.5, 0]$

A.1. $\alpha = 1$

In this case, wound field excitation is only used for weakening the PM excitation flux. The higher value of excitation current is obtained for $k_f = 0$, i.e., $I_{em} = |I_e| = \Phi_a / k_e$. In this case:

$$\begin{cases} k_{en} = \dfrac{k_e \cdot I_{em}}{\Phi_{e\,max}} = \dfrac{k_e \cdot (\Phi_a / k_e)}{\Phi_a} = 1 \\ \beta = \dfrac{V_m \cdot I_m}{V_{em} \cdot I_{em}} = \dfrac{V_m \cdot I_m}{R_e \cdot I_{em}^2} = \left(\dfrac{V_m \cdot I_m}{R_e}\right) \cdot \left(\dfrac{k_e}{\Phi_{e\,max}}\right)^2 = \beta_1 \end{cases} \tag{A.1}$$

A.2. $\alpha \in]1, 0.5]$

If the machine is designed with same maximum excitation flux $\Phi_{e\ max}$ and a hybridization ratio $\alpha \in]1, 0.5]$, it could be easily demonstrated that the maximum excitation current is still obtained for $k_f = 0$ (A.2).

$$\left.\begin{array}{l} k_f = 0 \Rightarrow \Phi_a + k_e \cdot I_e = 0 \Rightarrow I_e = -\Phi_a / k_e = -\alpha \cdot \dfrac{\Phi_{e\,max}}{k_e} \\ k_f = 1 \Rightarrow \Phi_a + k_e \cdot I_e = \Phi_{e\,max} \Rightarrow I_e = (\Phi_{e\,max} - \Phi_a) / k_e = (1-\alpha) \cdot \dfrac{\Phi_{e\,max}}{k_e} \end{array}\right\} \Rightarrow I_{em} = \alpha \cdot \frac{\Phi_{e\,max}}{k_e} \tag{A.2}$$

In this case:

$$\begin{cases} k_{en} = \dfrac{k_e \cdot I_{em}}{\Phi_{e\,max}} = \dfrac{k_e \cdot (\alpha \cdot \Phi_{e\,max} / k_e)}{\Phi_{e\,max}} = \alpha \\ \beta = \dfrac{V_m \cdot I_m}{V_{em} \cdot I_{em}} = \dfrac{V_m \cdot I_m}{R_e \cdot I_{em}^2} = \left(\dfrac{V_m \cdot I_m}{R_e}\right) \cdot \left(\dfrac{k_e}{\alpha \cdot \Phi_{e\,max}}\right)^2 = \dfrac{\beta_1}{\alpha^2} \end{cases} \tag{A.3}$$

A.3. $\alpha \in]0.5, 0]$

If the machine is designed now with same maximum excitation flux $\Phi_{e\ max}$, but with a hybridization ratio $\alpha \in]0.5, 0]$, it could be easily demonstrated that the maximum excitation current is obtained for $k_f = 1$ (A.4).

$$\left.\begin{array}{l} k_f = 0 \Rightarrow I_e = -\Phi_a / k_e = -\alpha \cdot \dfrac{\Phi_{e\,max}}{k_e} \\ k_f = 1 \Rightarrow I_e = (\Phi_{e\,max} - \Phi_a) / k_e = (1-\alpha) \cdot \dfrac{\Phi_{e\,max}}{k_e} \end{array}\right\} \Rightarrow I_{em} = (1-\alpha) \cdot \frac{\Phi_{e\,max}}{k_e} \tag{A.4}$$

In this case:

$$\begin{cases} k_{en} = \dfrac{k_e \cdot I_{em}}{\Phi_{e\,max}} = \dfrac{k_e \cdot \left((1-\alpha)\cdot \Phi_{e\,max}/k_e\right)}{\Phi_{e\,max}} = (1-\alpha) \\ \beta = \dfrac{V_m \cdot I_m}{V_{em} \cdot I_{em}} = \dfrac{V_m \cdot I_m}{R_e \cdot I_{em}^2} = \left(\dfrac{V_m \cdot I_m}{R_e}\right) \cdot \left(\dfrac{k_e}{(1-\alpha)\cdot \Phi_{e\,max}}\right)^2 = \dfrac{\beta_1}{(1-\alpha)^2} \end{cases} \tag{A.5}$$

Appendix B

The definition of base speed should be first recalled here; base speed is the maximum speed which could be reached while adopting the maximum torque control strategy, so its determination is equivalent to the determination of conditions allowing imposing the maximum torque. Torque expression, for non-salient poles synchronous machines, is given by:

$$T = p \cdot k_f \cdot \Phi_{e\,max} \cdot i_{0q} \tag{A.6}$$

From a first sight, it is easily understandable that the torque is maximized when k_f = 1 (maximum excitation flux), and when maximum value of i_{0q} is imposed. But rigorously, as regards to the adopted electrical circuits model, which includes iron losses, i_{0q} is dependent on k_f, and therefore the maximum (optimum) of the function T(k_f) should be determined in order to maximize the torque. Nevertheless, most electrical machines, for not saying all, are designed in order to minimize the iron loss, which are then modelled with a quite high value resistance R_f. The dependence of i_{0q} could then be neglected, in particular at relatively low speeds, and the torque is indeed maximized when k_f = 1 (maximum excitation flux), and when maximum value of i_{0q} is imposed.

In order to determine the maximum value of i_{q0} while respecting the armature current limit, relations between (i_{d0}, i_{q0}) and (i_d, i_q) should be first determined. These relations are given by equation (A.7).

$$\begin{cases} i_{0d} = \left[i_d + \left(L_d \cdot \omega \cdot i_q / R_f\right) - \left(L_d \cdot k_f \cdot \Phi_{e\,max} \cdot \omega^2 / R_f^2\right)\right] \Big/ \left[1 + \left(L_d \cdot \omega / R_f\right)^2\right] \\ i_{0q} = \left[i_q - \left(L_d \cdot \omega \cdot i_d / R_f\right) - \left(k_f \cdot \Phi_{e\,max} \cdot \omega / R_f\right)\right] \Big/ \left[1 + \left(L_d \cdot \omega / R_f\right)^2\right] \end{cases} \tag{A.7}$$

It could be noticed from equation (A.7), that if R_f is high, the dependence of i_{0q} on k_f could be effectively neglected. At the base speed and by imposing k_f = 1, the normalized value of i_{0q} is given by:

$$i_{0qn} = \left[i_{qn} - \left(L_{dn} \cdot i_{dn} / R_{fn}\right) - \left(1 / R_{fn}\right)\right] \Big/ \left[1 + \left(L_{dn} / R_{fn}\right)^2\right] \tag{A.8}$$

Once the maximum value of i_{0qn} is determined, the computation of V_{nmax} is straight forward. The Matlab scripts used in order to determine the maximum value of i_{0qn} and subsequently the value of V_{nmax} are given in following tables (Table A.1 and Table A.2).

Table A.1
Matlab script for the determination of Max(i_{0qn})

Start

Values of L_{dn}, R_{an} and R_{fn} should have been defined

$I_n = [0 : step_I : 1];$

$\psi = [-90 : step_\psi : 90];$

For i = 1 : length(I_n)

  For j = 1 : length(ψ)

    $i_{dn}(j) = -I_n(i) \cdot \sin(\psi(j));$

    $i_{qn}(j) = I_n(i) \cdot \cos(\psi(j));$

    $i_{0qn}(j) = f(i_{dn}(j), i_{qn}(j));$ (see equation (A.8), for the exact expression)

  End

  $[Y1(i),X1(i)] = \max(i_{0qn});$

  $i_{0qn1}(i) = i_{0qn}(X1(i));$

  $\psi_1(i) = \psi(X1(i));$

End

$[Y2,X2] = \max(i_{0qn1});$

$i_{0qnm} = i_{0qn1}(X2);$

End

Table A.2
Matlab script for the determination of V_{nmax} (this script is directly following the previous one)

Start

$i_{0qnm} = i_{0qn1}(X2);$

$I_{nOpt} = I_n(X2);$

$\psi_{Opt} = \psi_1(X2);$

$i_{dn1} = - I_{nOpt} \cdot \sin(\psi_{Opt});$

$i_{qn1} = I_{nOpt} \cdot \cos(\psi_{Opt});$

$i_{0dn} = h(i_{dn1}, i_{qn1});$ (see equation (A.7), for the exact expression)

$V_{dn} = (R_{an} \cdot i_{dn1} - L_{dn} \cdot i_{0qnm});$

$V_{qn} = (R_{an} \cdot i_{qn1} + 1 + L_{dn} \cdot i_{0dn});$

$V_{nmax} = \text{sqrt}(V_{dn}^2 + V_{qn}^2);$

End

Appendix C

This appendix contains three subsections, which will allow defining the values of:

1. i_{0dn0} allowing optimizing (minimizing) the total losses;
2. [i_{0dn1}, i_{0dn2}] for which $I_n \leq 1$;
3. [i_{0dn3}, i_{0dn4}] for which $V_n \leq V_{nmax}$.

C.1. Minimizing total losses

For a given (Torque, Speed) operating point, and a given value of excitation current, the losses are given by:

$$\begin{cases} P_{Cu} = R_a \cdot \left(i_d^2 + i_q^2 \right) + R_e \cdot I_e^2 \\ P_{Fe} = \left[\left(\rho \cdot L_d \cdot \omega \cdot i_{0q} \right)^2 + \left(L_d \cdot \omega \cdot i_{0d} + k_f \cdot \Phi_{e\,max} \cdot \omega \right)^2 \right] \Big/ R_f \end{cases} \tag{A.9}$$

For non-salient poles synchronous machines at a given excitation flux, the value of i_{0q} is given by:

$$i_{0q} = T \Big/ \left(p \cdot k_f \cdot \Phi_{e\,max} \right) \tag{A.10}$$

Using equations (A.9), (A.10) and relations between (i_d, i_q) and (i_{d0}, i_{q0}) (A.14), the total losses could be expressed as a function of i_{d0} as shown by equation (A.11).

$$P_{Cu} + P_{Fe} = \left(\begin{array}{l} R_a \cdot \left[\begin{array}{l} \left(i_{0d} + \left[L_d \cdot \omega \cdot T \Big/ \left(p \cdot k_f \cdot \Phi_{e\,max} \cdot R_f \right) \right] \right)^2 \\ + \left(T \Big/ \left(p \cdot k_f \cdot \Phi_{e\,max} \right) - \left[\left(k_f \cdot \Phi_{e\,max} + L_d \cdot i_{0d} \right) \cdot \omega \Big/ R_f \right] \right)^2 \end{array} \right] + R_e \cdot I_e^2 \\ + \left[\left(L_d \cdot \omega \cdot T \Big/ \left(p \cdot k_f \cdot \Phi_{e\,max} \right) \right)^2 + \left(L_d \cdot \omega \cdot i_{0d} + k_f \cdot \Phi_{e\,max} \cdot \omega \right)^2 \right] \Big/ R_f \end{array} \right) \tag{A.11}$$

It could be then shown that:

$$\frac{\partial \left(P_{Cu} + P_{Fe} \right)}{\partial i_{0d}} = 0 \Rightarrow i_{0d} = \frac{-\left(R_a + R_f \right) \cdot \left(L_d \cdot k_f \cdot \Phi_{e\,max} \right) \cdot \omega^2}{\left(R_a \cdot R_f^2 + \left(R_a + R_f \right) \cdot \left(L_d \cdot \omega \right)^2 \right)} \tag{A.12}$$

The normalized value of i_{0d}, given by equation (A.12), is i_{0dn0} shown in equation (4).

C.2. i_{0dn} for which $I_n \leq 1$

To find values of i_{0dn} allowing respecting the current limit constraint, the normalized armature current amplitude I_n should be expressed as a function of i_{0dn}. Knowing that:

$$I_n \leq 1 \Leftrightarrow I_n^2 \leq 1 \Leftrightarrow \left(i_{dn}^2 + i_{qn}^2 \right) \leq 1 , \tag{A.13}$$

and,

$$\begin{cases} i_d = i_{0d} - \left[\left(\omega \cdot \rho \cdot L_d \cdot \cdot i_{0q} \right) \Big/ R_f \right] \\ i_q = i_{0q} + \left[\left(\omega \cdot k_f \cdot \Phi_{e\,max} + \omega \cdot L_d \cdot i_{0d} \right) \Big/ R_f \right] \end{cases}, \tag{A.14}$$

by combining these two equations (equation (A.14) should be used in its normalized version) and replacing i_{0qn} by its expression deduced from equation (A.10), a quadratic equation of i_{0dn} is obtained (5). It should be recalled that these developments are only true for non-salient poles synchronous machines.

It should be noticed that $A_I > 0$, which implies:

$$I_n \leq 1 \Leftrightarrow i_{0dn} \in \left[i_{0dn1},\ i_{0dn2} \right] . \tag{A.15}$$

C.3. i_{0dn} for which $V_n \leq V_{nmax}$

To find values of i_{0dn} allowing respecting the voltage limit constraint, the normalized armature voltage amplitude V_n should be expressed as a function of i_{0dn}. Knowing that:

$$V_n \leq V_{n\,max} \Leftrightarrow V_n^2 \leq V_{n\,max}^2 \Leftrightarrow \left(v_{dn}^2 + v_{qn}^2\right) \leq V_{n\,max}^2\,, \tag{A.16}$$

and,

$$\begin{cases} v_d = R_a \cdot i_d - \omega \cdot \rho \cdot L_d \cdot \cdot i_{0q} \\ v_q = R_a \cdot i_q + \omega \cdot \left(k_f \cdot \Phi_{e\,max} + L_d \cdot i_{0d}\right) \end{cases}, \tag{A.17}$$

by combining these two equations (equation (A.17) should be used in its normalized version) and replacing i_{0qn} by its expression deduced from equation (A.10), a quadratic equation of i_{0dn} is obtained (6). It should be recalled that these developments are only true for non-salient poles synchronous machines.

It should be noticed that $A_V > 0$, which implies:

$$V_n \leq V_{n\,max} \Leftrightarrow i_{0dn} \in \left[i_{0dn3},\ i_{0dn4}\right]. \tag{A.18}$$